Macedonian Journal of Chemistry and Chemical Engineering, Vol. **42**, No. 1, pp. 103–114 (2023)

MJCCA9 – 877

ISSN 1857-5552
e-ISSN 1857-5625

Received: March 22, 2023
Accepted: April 4, 2023

DOI: doi.org/10.20450/mjcce.2023.2677
Original scientific paper

VOLTAMMETRIC EXAMINATION OF HYDROQUINONE AT ORDINARY AND NANO-ARCHITECTURE PLATINUM ELECTRODES

Ahmed A. Al-Owais[1], Ibrahim S. El-Hallag[*2], Elsayed El-Mossalamy[3]

[1]*Chemistry Department, Faculty of Science, King Saud University, Saudi Arabia*
[2]*Chemistry Department, Faculty of Science, Tanta University, Tanta, Egypt*
[3]*Chemistry Department, Faculty of Science, Benha University, Benha, Egypt*
i.elhallag@yahoo.com

The electrochemical behavior of hydroquinone was examined experimentally using cyclic voltammetry, convolution transform, and deconvolution transform at clean ordinary and nanostructured mesoporous platinum electrodes in 1 mol/l $HClO_4$. The cyclic voltammogram of hydroquinone (HQ) at an ordinary Pt electrode displays an anodic peak at 0.610 V and a cathodic peak at 0.117 V, with a scan rate of 50 $mV \cdot s^{-1}$. Excellent linearity was recorded between the anodic or cathodic peak currents of hydroquinone and the square root of the scan rate ($\upsilon^{1/2}$). The anodic and cathodic peak potential separation (ΔE_p) was found to be 463 ± 3 mV *vs.* the saturated calomel electrode (SCE). It was noted that the value of peak potential separation increased with increasing the scan rate. The type of electrode reaction at both platinum electrodes in 1 mol/l $HClO_4$ was examined and discussed. The electrochemical parameters and the nature of the mechanistic pathway of the investigated HQ were determined experimentally and ascertained via a numerical simulation method.

Keywords: hydroquinone; cyclic voltammetry; convolution transform; deconvolution transform; numerical simulation

ВОЛТАМЕТРИСКО ИСПИТУВАЊЕ НА ХИДРОХИНОН СО ОБИЧНИ И СО ПЛАТИНСКИ ЕЛЕКТРОДИ СО НАНО-АРХИТЕКТУРА

Електрохемиското однесување на хидрохинон беше експериментално испитано со примена на циклична волтаметрија, трансформација на конволуција и трансформација на деконволуција на обични и на платински мезопорозни наноструктурирани електроди во 1 mol/l $HClO_4$. Цикличниот волтамограм на хидрохинон (HQ) на обична Pt електрода покажува аноден пик на 0,610 V и катоден пик на 0,117 V со брзина на скенирање од 50 $mV \cdot s^{-1}$. Беше регистрирана одлична линеарност меѓу анодната и катодната струја на хидрохинон и квадратниот корен од брзината на скенирање ($\upsilon^{1/2}$). Разделувањето на потенцијалот (ΔE_p) меѓу анодниот и катодниот пик изнесуваше 463 ± 3 mV во однос на заситена каломелова електрода (SCE). Забележано е дека вредноста на разделување на потенцијалот на пикот се зголемува со зголемување на брзината на скенирање. Испитан и дискутиран е типот на електродната реакција на двете платински електроди во 1 mol/l $HClO_4$. Електрохемиските параметри и природата на механизмот на испитуваниот HQ се определени експериментално и потврдени со методот на нумеричка симулација.

Клучни зборови: хидрохинон; циклична волтамтерија; трансформација на конволуција; трансформација на деконволуција; нумеричка симулација

1. INTRODUCTION

The widespread interest in replacing fossil fuels with renewable energy sources is a challenging task motivated by a need for energy independence and carbon footprint reduction. The cost of wind and photovoltaic electricity is still decreasing and will be integrated even more in a future fully renewable-based utility grid. Recently, organic aqueous flow batteries have been proposed as a low-cost alternative to the present metal-based redox flow battery (RFB) technology.[1–4] Green and renewable energy technologies, such as solar and wind energy technologies, serve as a rational way to reduce greenhouse gases; however, this kind of power generation requires the development of energy storage facilities.[5] Now, redox flow batteries (RFBs) have been introduced for energy storage.[6–8] The energy of a redox flow battery depends on the electrolyte volume and the electroactive material concentration, whereas its power is related to the electrode size, the reactions involved, and the cell design.[9,10] Since 1970, a number of RFBs, such as the vanadium-vanadium redox flow battery, have been fabricated and developed.[11–13] Among various redox flow batteries, low-pollution materials have become more desirable by virtue of their environmental effects. Organic materials that do not include heavy metals are particularly interesting. These materials have recently attracted attention as alternative active materials for redox flow batteries.[14,15] Using 1,4-hydroquinone and some of its derivatives as electroactive materials for cathodic or anodic electrodes in general rechargeable batteries is practically difficult due to certain problems, such as the dissolution of these organic compounds in the electrolytes, instability of intermediate radical species, low electrical conductivity, and their high capacity for sublimation.[16] For these reasons, these compounds have not been used as electroactive battery materials in most cases. Instead, they are suitable for redox flow batteries due to their high solubility. In fact, redox flow batteries are energy storage devices in which the anolyte (the electrolyte in the vicinity of the anode) and the catholyte (the electrolyte in the vicinity of the cathode) reactions of an electrochemical cell occur by means of redox species present in the solution.[17] In the literature, a large capacity is reported for some hydroquinone derivatives when used as positive electrolyte materials in flow redox batteries.[17] In a redox flow battery, RFB, both reduced and oxidized forms of the anolyte and catholyte electroactive materials are soluble. In a hybrid redox flow battery, HRFB, both reduced and oxidized forms of the electroactive species are soluble in one of the half-cells. For the other half-cell, however, at least one of the reduced or oxidized species of electroactive materials is not soluble and forms a different phase.[9] Among the various known organic depolarizers, research on the quinone-hydroquinone redox system has received a lot of attention.[18–20] The best organic depolarizers can be classified into four types: (i) nitro compounds (RNO_2); (ii) positive halogen compounds (ROX and RNX); (iii) halogen addition compounds (R, NX); and (iv) peroxides (ROOR). Among these compounds, nitro compounds (e.g., *m*-dinitrobenzene) theoretically possess 1.91 $Ah \cdot g^{-1}$ output capacity. This is primarily due to the transfer of many electrons during the reduction process.[21,22] These compounds do not, however, exhibit good reversible behavior, nor has it been possible to realize in practice the capacity that is expected from them. As is well known, oxidation and reduction reactions in organic chemistry are irreversible by nature. An exception to this is the group of compounds involving quinone-benzonoid reaction equilibrium. The quinone-hydroquinone redox reaction is considered one of the best reversible systems.[23] Earlier work on the quinone-hydroquinone system indicates that quinone, or its substituted compounds, is considered a promising candidate for use in primary as well as secondary batteries.[24,25] Capson and Parsons selected *N*,*N*'- dimethylformamide (DMF) as an ideal test solvent for the reduction of p-benzoquinone using six different working electrodes, viz., Pt, Pd, Ir, Rh, Au, and Hg.[25]

The redox reaction of quinones in buffered water is well described as an overall 2 e^-, 2 H^+ reduction to make the hydroquinone. A much better description of the overall reaction in unbuffered water is as a 2 e^- reduction to make the strongly hydrogen-bonded quinone dianion, which will exist in water as an equilibrium mixture of protonation states.[26] The electrochemically reduced forms of the hydroxylated CoQs have higher antioxidative potential and can bind and transport Ca^{2+} across artificial biomimetic membranes.[27] The redox chemistry of coenzyme Q members in non-aqueous aprotic organic solvents can be described by two consecutive one-electron transfer steps; a more complex situation exists in the voltammetry of coenzyme Qs performed in aqueous media.[28] Intensive voltammetric and spectroscopic studies of coenzyme Q systems in buffered and non-buffered aqueous media have revealed that hydrogen bonding between electrochemically created CoQ species and the water molecules plays an im-

portant role in stabilizing electrochemically generated species of these systems.[28] The discovery of metal-based nanoparticles and their application as modifiers of different electrode surfaces was the next step forward in the era of the developing voltammetric biosensors.[29] However, a real revolution in improving the overall performance of commercial working electrodes and their intensive application in developing voltammetric bio-sensors happened some 20 years ago. During a presentation on some recent achievements of protein-film voltammetry (PFV) some novel protocols that contribute to better communication between redox enzymes and the working electrode were explained.[30] In addition, the reported results give a short overview of several novel voltammetric techniques derived from the perspective of square-wave voltammetry. These techniques seem to be promising tools for application in PFV.[30] The advances in square-wave voltammetry for analytical purposes as well as for studying electrode mechanisms and kinetics and for the quantitative determination of various compounds, such as medications, biomolecules, environmental pollutants, and antioxidants, were reviewed and reported.[31]

The main objective of this manuscript is to study, for the first time, the kinetic and mechanistic pathways of hydroquinone electro-oxidation in acid solution ($HClO_4$) at an ordinary and a nanostructured mesoporous Pt electrode via cyclic voltammetry, convolution-deconvolution transforms, and numerical simulation methods. It was found that the convolution-deconvolution transforms and the numerical simulation method provide simple and accurate tools for calculation, confirmation of the electrochemical parameters of hydroquinone, and understanding the mechanistic pathway of the electrode reaction.

2. EXPERIMENTAL

2.1. *Chemical reagents*

Fluka provided hydrogen hexachloroplatinate(IV) hydrates HCPA (99.9 %), polyethylene (10), and cetylether surfactant ($C_{16}EO_8$, 99 %, $C_{16}H_{33}(OCH_2CH_2)_{10}OH$. $HClO_4$; 1,4-hydroquinone (HQ), was purchased from Aldrich. De-ionized and filtered water with a resistivity higher than 18 M Ohm/cm was taken from an Elga water purification system. Argon (BOC, UK) was employed to deaerate the electrolyte solutions for half an hour before each experiment.

2.2. *Instrumentation*

To investigate the redox behavior of the hydroquinone/quinone redox couple, we performed three-electrode tests for data capture using cyclic voltammetry measurements (CV). A conventional three-electrode cell using a micro-Autolab type III system (Eco Chemie, NL) was used for these electrochemical studies. The reference electrode was a saturated calomel electrode (SCE), and the counter electrode was about 1 cm^2 of platinum gauze. The working electrode was a 1 mm diameter Pt disc sealed in glass with a surface area of $7.85 \cdot 10^{-3}$ cm^2. The potential window varied from –0.2 V to 1.0 V vs. SCE. The scan rates used in this study were in the range of 20 $mV \cdot s^{-1}$ – 1000 $mV \cdot s^{-1}$. All electrochemical experiments were carried out in 1 mol/l $HClO_4$ at room temperature 23 ± 2 ºC. The numerical simulation method was used to know the exact nature of electrode reactions and to confirm the determined electrochemical and chemical parameters such as diffusion coefficient (D), the heterogeneous rate constant of charge transfer (k_s), redox potential (E^o), homogeneous chemical rate constant (k_c), and the symmetry coefficient (α).

3. RESULTS AND DISCUSSION

Voltammetric measurements of HQ at a standard Pt electrode were performed in a 1.0 M $HClO_4$ solution to confirm the simple proton transfer and stability of the redox process in acidic media. The CV curves, recorded at a 50 mV s^{-1} scan rate in the presence of 5 mM HQ in 1.0 M $HClO_4$, at an ordinary Pt electrode are shown in Fig. 1a.

It was noticed that the cyclic voltammograms of hydroquinone exhibit oxidative and reductive peak positions of 0.610 and 0.117 V vs. SCE, respectively, with a peak potential distance (ΔE_p) of 0.493 V. In the reverse sweep, the cathodic peak coupled with the anodic peak was absent, which means that the electrode behavior of HQ in the anodic direction apparently proceeds as an EC mechanism. The value of half-peak width (E_p–$E_{p/2}$) listed in Table 1 indicates that the rate of charge transfer during oxidation of HQ at an ordinary Pt electrode is slow and proceeds as a sluggish electron transfer kinetic process. These results are consistent with the fact that HQ's slow electrode processes at the Pt electrode's clean surface are slow processes in nature.[32]

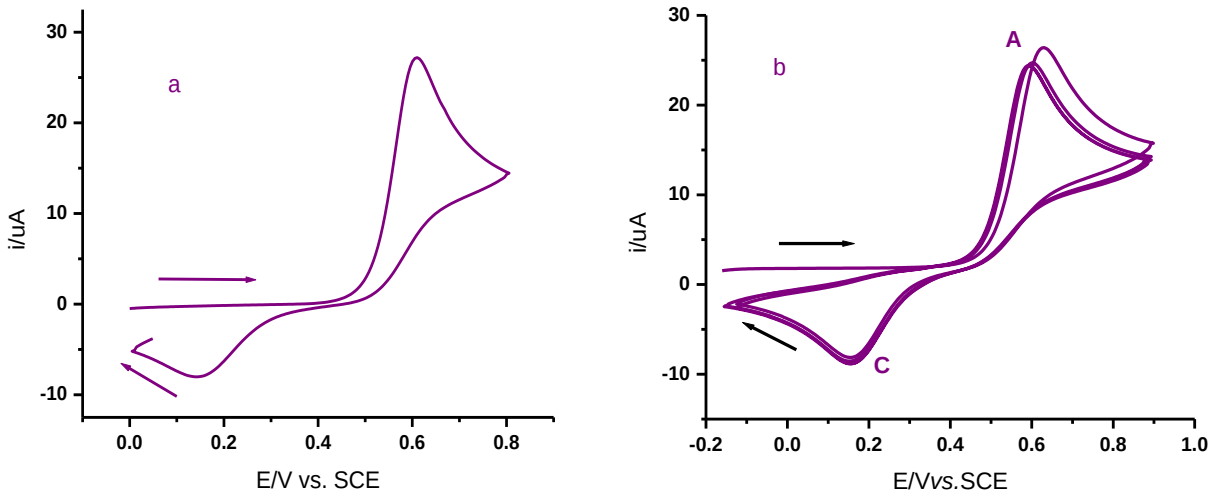

Fig. 1. Single sweep **(a)** and three sweep cyclic voltammograms
(b) at a scan rate of 50 mV·s^{-1} for 5 mM HQ in 1.0 M $HClO_4$ at an ordinary Pt electrode

Three sweeps of the cyclic voltammograms at a clean Pt electrode with 5 mM HQ at 50 mV s^{-1} scan rate in 1.0 M $HClO_4$ are shown in Figure 1b. It was observed that after the first scan, there was a decrease in peak height. This decrease in peak height following the first sweep is due to the difference in the active surface area between the fresh, neat Pt surface and the new surface generated due to the formation of a thin layer of HQ oxidation products on the Pt surface. After the first sweep, the current remains constant for over 50 cycles, indicating the stability and fouling resistance of the electrode for the oxidation of hydroquinone. In addition, the shift of E^f_p to less positive values after the first sweep can be attributed to the higher catalytic activity of the thin layer formed from HQ oxidation products than that of the neat Pt surface. From Table 1, it was noticed that the values of peak current increase with increasing the scan rate, and the anodic peak potentials shift to more positive values while the cathodic peak potentials in the reverse scan shift to less positive values. In addition, the magnitudes of half-peak width reflect the slow nature of the rate of electron transfer. As noticed in Figure 1b, the absence of the counter cathodic peak coupled with the anodic peak and the non-existence of an anodic peak coupled with the cathodic peak (c) exclude the EC mechanism and ECE mechanism, respectively. Further, the ratio of i_p^b /i_p^f is less than unity, confirming the exclusion of the probability of presenting a simple slow electron transfer mechanism (ET). As a result, the electrode reaction pathway does not follow a simple electron transfer (ET) or a charge transfer (EC or ECE) process.

T a b l e 1

The wave parameters of the investigated HQ calculated from CV at (a) ordinary and (b) nano-architecture Pt electrodes at various scan rates

υ,Vs^{-1}	E_p^f/mV	E_p^b/mV	E_p-$E_{p/2}$ /mV	ΔE_p/ mV	i_pf ·10^6/A	i_pb·10^6/A	i_pb/i_pf
0.10	637 [a]	97	90	540	26.80	20.20	0.75
	582[b]	465	43	117	36.42	25.39	0.69
0.20	656[a]	88	97	568	37.90	22.0	0.58
	597[b]	454	48	143	50.93	32.68	0.64
0.50	689[a]	45	103	644	58.52	41.00	0.70
	611[b]	454	54	157	77.31	45.40	0.58
1.0	698[b]	36	107	662	80.75	56.6	0.70
	623[a]	456	59	167	108.25	64.49	0.59

3.1. *Effect of scan rate*

As shown in Figure 2, when the scan rate increases, the potential separation between the anodic and cathodic peaks increases. The anodic peak shifts towards more positive potentials, while the cathodic peak shifts towards less positive potentials. Overall, the current ratios (i_p^c/i_p^a) are less than unity in the cases of mesoporous Pt electrodes and ordinary Pt electrodes. The ratio at the mesoporous electrode is greater than that at the ordinary electrode. This behavior could be explained by the fact that the chemical step that follows the oxidative process at the ordinary Pt electrode is faster than that at the mesoporous electrode. Furthermore, at a scan rate of 50 $mV \cdot s^{-1}$, the peak separation between the anodic and cathodic peak potentials is 493 and 793 mV at ordinary and mesoporous platinum electrodes, respectively, which is greater than 59 mV/n and indicates that electron transfer in the system is slow in the case of a clean Pt electrode and moderately fast in the case of a mesoporous Pt electrode.

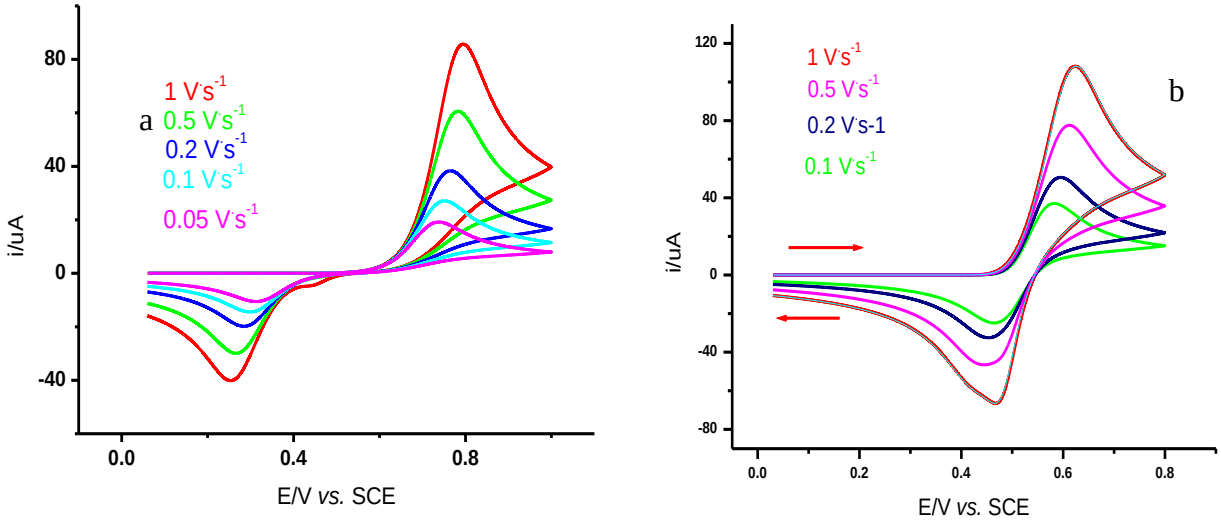

Fig. 2. Cyclic voltammetry of 5 mM HQ at different sweep rates in 1.0 M $HClO_4$ at **(a)** ordinary and **(b)** nanostructured mesoporous Pt electrodes

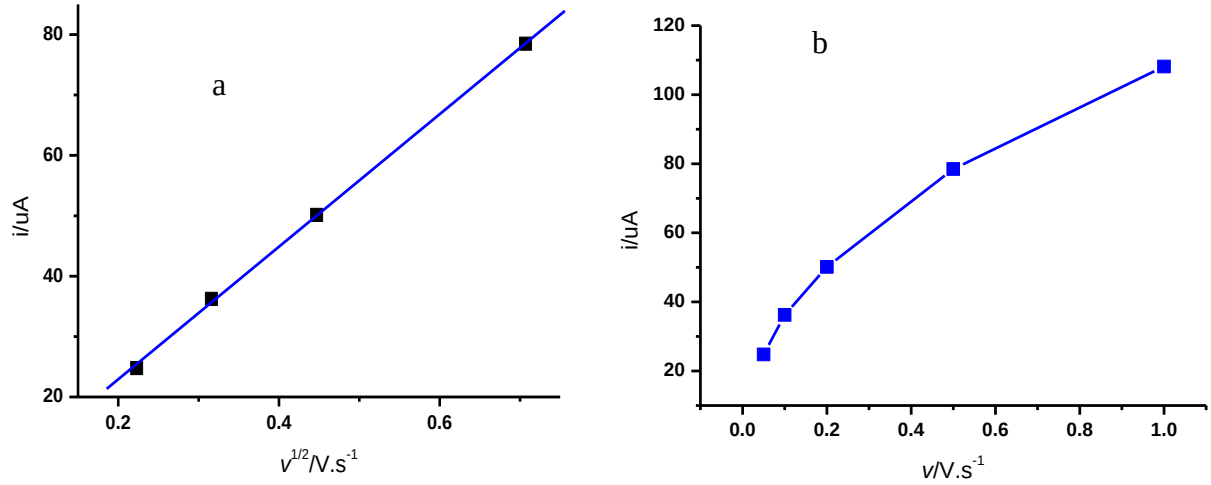

Fig. 3. Variation of peak current (i_{pa}) with the square root of scan rate (v)1/2 **(a)** and scan rate (v) **(b)** for 5 mM HQ in 1.0 M HClO4 at a nanostructured mesoporous Pt electrode

The effect of the potential scan rate on the electrochemical process was investigated to better understand electrode behavior and the reversibility of electrode reactions. Figure 3 shows anodic peak current extracted from a cyclic voltammogram of 5 mM HQ in 1.0 M $HClO_4$ at a nanostructured mesoporous Pt electrode using the square root of scan rate (v) and scan rate (v). It was discovered that as the scan rate was increased, the oxidation peak current produced a good linear relationship with the square root of the scan rate (Fig. 3a). In contrast, the plot deviated from linearity in the case of the scan rate. The observed behavior confirms that the mesoporous Pt electrode reaction is controlled by the diffusion nature of mass transport of HQ species in 1.0 M $HClO_4$. The values of the diffusion coefficient at ordinary and mesoporous Pt electrodes were calculated from the slope of i_p vs. $\upsilon^{1/2}$ and are shown in Table 2. It was found that the peak potential separation (ΔE_p) increases with increasing the scan, as shown in Figure 4. This indicates that the rate of heterogeneous electron transfer for the redox reaction of HQ in this study can be considered to be a quasi-reversible process at the nanostructured mesoporous Pt electrode and slow at the clean Pt electrode.

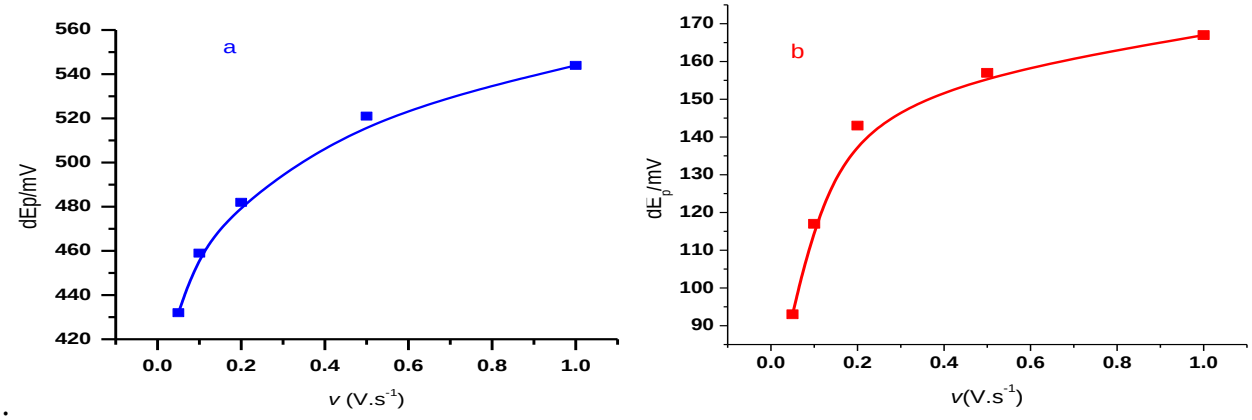

Fig. 4. Variation of peak potential separation (ΔE_p) as a function of applied scan rate (v) of HQ in 1.0 M $HClO_4$ at ordinary (a) and nanostructured mesoporous (b) Pt electrodes

As previously stated, increasing v generally increases current and causes the position of peak potential to shift to more positive values in the forward direction of the scan. Although i_{pa} (anodic peak current) is strongly related to E_p, the relationship has rarely been quantified. Plotting i_{pa} against E_{pa}, as shown in Figure 5, is one method of analyzing the potential shift.[25] The potential extrapolation to zero current on each straight line should be close to the redox potential (E^o).[25] As shown in Figure 5, the values of intercept for the anodic peaks at the ordinary and mesoporous Pt electrodes are 0.752 V and 0.580 V, respectively. For reduction peaks, the values of intercept at the ordinary and mesoporous Pt electrodes were exhibited at 0.315 V and 0.480 V, respectively, which are very close to the values of redox potential cited in Table 2. The values of the oxidative and reductive transfer coefficients (α) were calculated from the following relationship[33] (Eq. 1) and listed in Table 2:

$$E_p - E_{\frac{p}{2}} = {}^{48}/_{\alpha n_a} \qquad (1)$$

where $E_p - E_{p/2}$ is the half peak width. Again, the values of diffusion coefficients (D) were calculated from the relationship between the peak current, i_p, and the square root of the scan rate, $\upsilon^{1/2}$,[33] and cited in Table 2. Furthermore, as established in the literature and shown in Table 2,[34] the values of the heterogeneous rate constant, k_s, were calculated from the half peak width $E_p - E_{p/2}$ versus the dimensionless parameter (ψ).

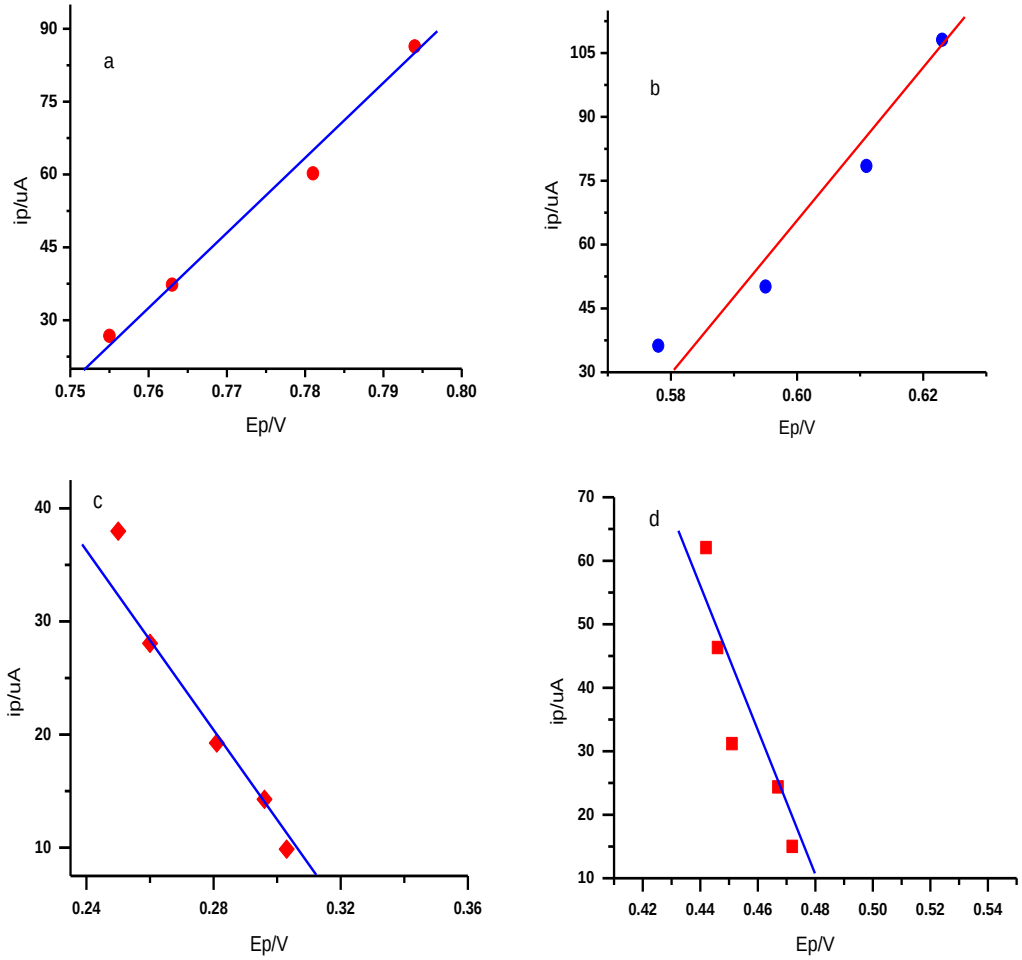

Fig. 5. Plot of i_p vs. E_p of the oxidative peak for HQ at an ordinary Pt electrode **(a)**, at a mesoporous Pt electrode **(b)**, for the reductive peak at an ordinary Pt electrode **(c)**, and at a mesoporous Pt electrode **(d)** in 1M $HClO_4$ at various scan rates

3.2. *Convolutive voltammetry*

Convolution voltammetry consists essentially of a voltammetric, chronoamperometric, or chronocoulometric experiment followed by a mathematical process of transformation-convolution. The technique delivers quantities directly related to the concentration of electroactive species (C_A) at the electrode surface (instead of the flux of a compound, as in the case of the original techniques), and it is rather insensitive to i_R drop.

For electroactive species A, which behaves as a simple electron transfer mechanism, Fick's Second Law is written as follows:[33]

$$\left[\frac{\partial C_A}{\partial t}\right]_x = D_A\left[\frac{\partial^2 C_A}{\partial x^2}\right]_x \qquad (2)$$

Solving the above equation at the electrode surface provides

$$I_1(t) = \left(C_A{}^b - C_A{}^s\right).\left[nFSD_A{}^{\frac{1}{2}}\right] \qquad (3)$$

where C^b_A and C^s_A are the bulk and surface concentrations, respectively.

The surface electrode area is referred to by the symbol S, and $I_1(t)$ is the semi-integration of current and is defined as shown in Equation (4):[34]

$$I_1(t) = \pi^{-1/2}\int_0^t [i(u)/(t-u)^{1/2}]\,du \qquad (4)$$

where $i(u)$ is the current at time u and t is the total elapsed time.

$I_1(t)$ gives its limiting value, I_{lim},

$$I_{lim} = nFSC\sqrt{D} \qquad (5)$$

under the condition of pure diffusion-control [i.e., $C_{(0,t)} = 0$]. Therefore, semi-integration converts the cyclic curve (i–E) to the $I(t)$ –E steady-state curve, and, in some cases, this is more adjustable for data analysis.[34]

The evaluation of $I_1(t)$ was performed via the following algorithms:[35]

$$I(t) = I(k\Delta t) = \frac{1}{\sqrt{\pi}} \sum_{j=1}^{j=k} \frac{\Gamma\left(k-j+\frac{1}{2}\right)}{(k-j)} . \Delta t^{\frac{1}{2}} i(j\Delta t) \quad (6)$$

At equally spaced intervals of Δtm, the current is represented by $I(j\Delta t)$, and $\Gamma(x)$ is the Gamma function of x. The I_1 convolution curve of the examined HQ under consideration at an ordinary Pt electrode is indicated in Figure 6a, which shows a distinct separation between the forward and backward sweep when it is driven in the reverse direction.[35–37] This behavior can be attributed to a moderate rate of electron transfer. In addition, the unreturning of the backward scan of I_1 convolution to a zero value confirms and supports the existence of a chemical step in the electrode pathway of HQ in 1 mol/l $HClO_4$ at an ordinary Pt electrode surface.

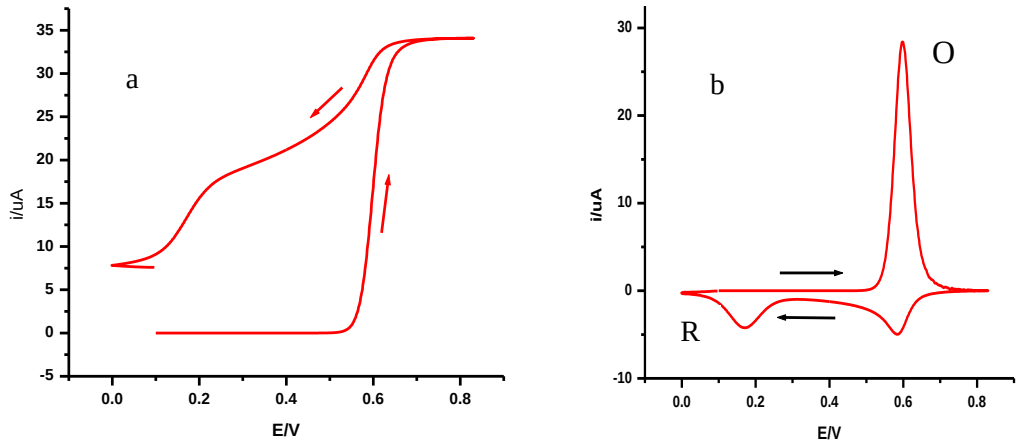

Fig. 6. Convolution voltammogram of HQ in 1.0 M $HClO_4$ at an ordinary Pt electrode **(a)** and deconvolution at the same ordinary Pt electrode **(b)**

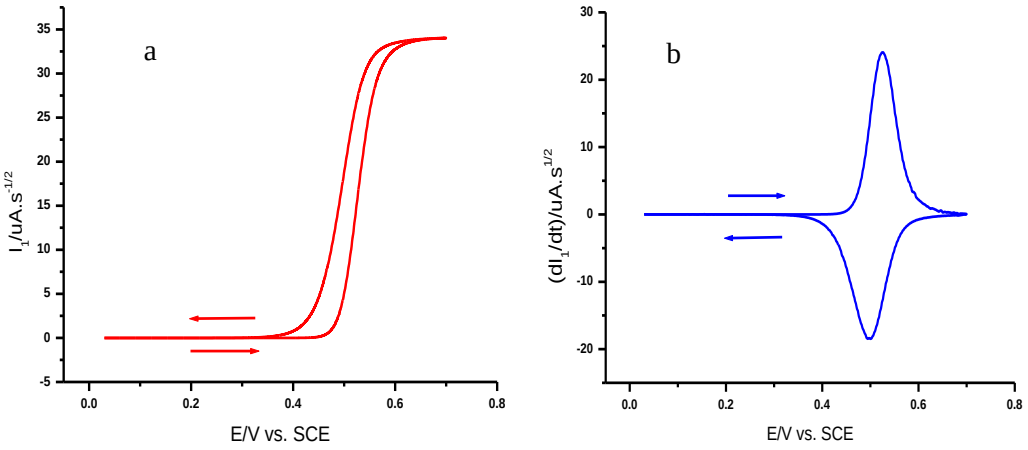

Fig. 7. Convolution voltammogram of HQ at a mesoporous Pt electrode **(a)** and deconvolution voltammogram at a mesoporous Pt electrode **(b)** in 1.0 M $HClO_4$

The convolution voltammogram curve of the examined HQ at mesoporous Pt electrode is indicated in Figure 7a, which shows less potential separation of the distance between the forward and backward scan than that observed at the ordinary Pt electrode (Figure 6a). This indicates that the rate of electron transfer at a mesoporous Pt electrode is faster than that obtained at an ordinary Pt electrode.[36,37]

Deconvolution voltammetry is performed as a semi-differentiation of the current ($d\ I_1\ /dt$) with respect to the applied potential and is defined as follows:[36]

$$(dI_1/dt) = nFSC\sqrt{D}a\zeta/(1+\zeta)^2 \quad (7)$$

The symbols a and ζ are defined as follows:

$$a = n\nu F/RT \quad (8)$$

$$\zeta = \exp\left[\frac{nF}{RT(E-E^0)}\right] \quad (9)$$

The deconvolution voltammetry curve at an ordinary Pt electrode with v = 50 mV·s^{-1} is displayed in Figure 6b. The half-width of the deconvoluted peak ($w^{p/2}$) is written as[34]

$$w^{p/2} = 2.94\,RT/\alpha n_a F \qquad (10)$$

for a rate-controlled process, where n_a is the number of electrons participating in the rate-determining step, R is the universal gas constant, T is the absolute temperature, and F is the Faraday constant. The half-width of the deconvoluted peak at half the height of the peak ($w^{p/2}$) was measured experimentally and found to be 101 ± 2 mV, indicating the slow nature of electron transfer of HQ at an ordinary Pt electrode surface. The values of the symmetry coefficient (α) were calculated via Eq. (10) and listed in Table 2. In addition, the distance between the peak locations of the oxidative peak (O) and the reductive peak (R) is large, confirming that the reduction peak of HQ at the Pt electrode is not coupled with the oxidation process. The slight displacement of the maximum and minimum deconvolution peaks at the mesoporous electrode supports the quasi-reversibility of electron transfer in the oxidative processes. The values of the electrochemical parameters determined experimentally are listed in Table 2.

The height of the deconvolution voltammetric peak (e_p) was used for the calculation of the diffusion coefficient (D) via Eq. (11)[38,39] and put in Table 2.

$$e_p = \frac{\alpha n^2 F^2 v D^{1/2} C^{bulk}}{3.367RT} \qquad (11)$$

where v is the scan rate, the symbol e_p is the height of the forward deconvolution peak (in amperes), and the remaining parameters have their known meanings. The determined values of the diffusion coefficient using Eq. (11) are cited in Table 2. In addition, the number of electrons involved in the mechanistic pathway was calculated from equation (12).

$$n = \frac{0.086 e_p}{I_{lim}\alpha v} \qquad (12)$$

The calculated number of electrons involved in the electrode reaction, n, was found to be 2.01 for both anodic and cathodic reactions using Eq. (12). As demonstrated, the above equation provides a successful and straightforward method for calculating the number of electrons consumed in the electrode reaction without knowing the electrode surface area. From the above results, it was noted that the I_1 *vs.* E and (dI_1/dt) *vs.* E curves were easier to elucidate and confirmed the nature of the electrode reaction.

The data obtained in this work are compared with that established in the literature[40–43] and summarized in Table 3, which indicates the good catalytic activity of mesoporous Pt electrodes.

T a b l e 2

Values of the electrochemical parameters obtained at the ordinary and mesoporous platinum electrodes

k_{sOx} /ms^{-1}	k_{sRed}m.s^{-1}	E^0_{Ox}/V	E^o_{Red}/V	D_{Ox} m^{2}s^{-1}	D_{Red}m^{2}s^{-1}	α_{Ox}	α_{Red}	k_{COx} s^{-1}	k_{CRed} s^{-1}
[a] 4.4e–5	3.8e–5	0.750	0.310	5.3e–9	5.12e–9	0.36	0.33	3.52	2.41
[b] 6.1e–7	5.3e–7	0.683	0.483	4.2e–9	3.90e–9	0.34	0.31	6.91	5.81

[a] values obtained at a mesoporous Pt electrode and [b] values obtained at a ordinary Pt electrode

T a b l e 3

Compares data from the literature with that obtained in our study

Electrode type	Solution conditions	ΔE_p/mV	i_{pb}/i_{pf}	D cm^{2}s^{-1}	k_s, cms^{-1}	Ref.
(PGDIL)–TiO_2/Au	0.1M TBAP/acetonitrile	533	0.43	$2.77\cdot10^{-5}$	–	40
GCE	0.3M Mg perchlorate	255	0.92	–	–	41
Au disk	0.2M TBAP/ acetonitrile	547	0.81	–	–	42
Boron doped diamond	H_2SO_4 soln.	565	–	–	–	43
Mesoporous Pt	1M $HClO_4$	117	0.69	$5.3\cdot10^{-5}$	$4.4\cdot10^{-4}$	[this work]

4. NUMERICAL SIMULATION

The numerical simulation method is an important and successful tool for knowing the type of mechanistic pathway of electrode reactions and obtaining the kinetic parameters theoretically.[38,39] The transfer coefficients, E^0, D, and k_s, for anodic and cathodic electrode mechanisms were estimated experimentally and ascertained via numerical simulation.[35,36] The best fit between experimental and theoretical curves consists of finding the electrochemical parameters that exhibit the fewest differences between the numerically simulated curves and the experimental plots. As shown in Figure 8, there is good matching between the theoretical and the captured experimental voltammograms, confirming the validity of the proposed mechanistic pathway of the electrode reaction, which is proposed to proceed as an ECEC mechanism, and the accuracy of the electrochemical parameters calculated experimentally.

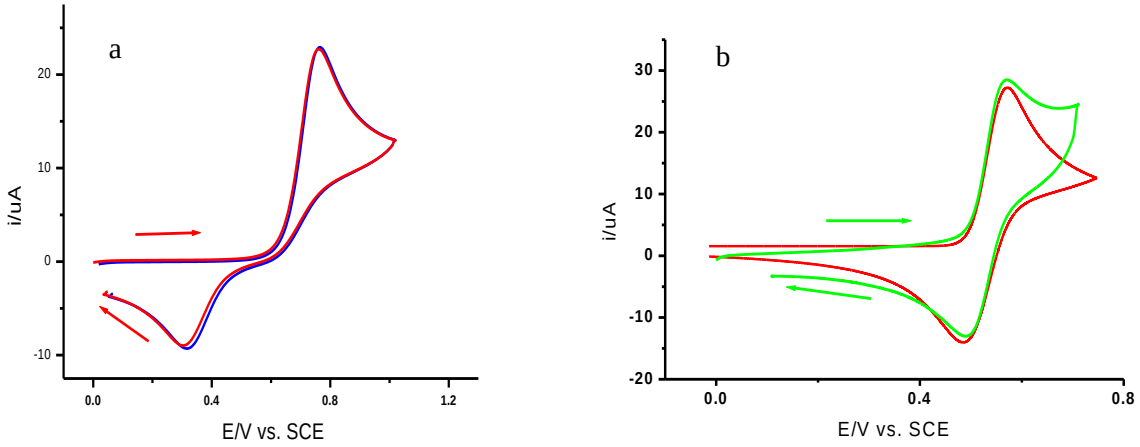

Fig. 8. Simulated and experimental ECEC cyclic voltammograms of HQ at an ordinary Pt electrode **(a)** and a mesoporous Pt electrode **(b)**

5. CONCLUSION

The redox behavior of HQ at an ordinary Pt electrode was demonstrated, and a nanostructured mesoporous platinum film was electrochemically deposited from a hexagonal liquid crystalline template. The mesoporous platinum electrode exhibited excellent electrocatalytic properties, activity, and reversibility toward the oxidation of the HQ system. The oxidation and reduction peak separation (ΔE_p) decreased from 540 to 117 mV vs. SCE for HQ at ordinary and mesoporous platinum electrodes, respectively. The electrocatalytic enhancement, stability, and selectivity for HQ oxidation demonstrate the potential use of a nanostructured mesoporous film for further investigation. In the case of a mesoporous platinum electrode, the cyclic voltammogram exhibits one anodic peak in the forward scan of potential and one cathodic peak in the reverse scan. On the basis of the electrochemical behavior, the suggested mechanism is an ECEC scheme for the electrochemical oxidation of HQ in 1.0 M $HClO_4$ at both electrodes. Numerical simulation was used for confirmation of the proposed electrode reaction and the electrochemical parameters measured experimentally.

Acknowledgements. This project was supported by King Saud University, Deanship of Scientific Research, College of Science, Research Center.

REFERENCES

(1) Huskinson, B.; Marshak, M.; Suh, C.; Er, S.; Gerhardt, M.; Galvin, C.; Chen, X.; Guzik, A.; Roy, G.; Gordon, R.; Aziz, M., A metal-free organic–inorganic aqueous flow battery, *Nature* **2014**, *505*, 195. https://doi.org/10.1038/nature12909

(2) Lin, K.; Chen, Q.; Gerhardt, M.; Tong, L.; Kim, S.; Eisenach, L.; Valle, A.; Hardee, D.; Gordon , R.; Michael, J.; Aziz, M. M., Alkaline quinone flow battery. *Science Magazine* **2015**, *349*, 1529. doi:10.1126/ science.aab303

(3) Yang, B.; Hoober-Burkhardt, L.; Wang, F.; Prakash, G.; Narayanan, S., An inexpensive aqueous flow battery for large-scal electrical energy storage based on water-soluble organic redox couples. *J. Electrochem. Soc.* **2014**, *161*, A1371. doi:10.1149/2.1001409JES

(4) Janoschka, T.; Martin, N.; Martin, U.; Friebe, C.; Morgenstern, S.; Hiller, H.; Hager, M .; Schubert, U., An aqueous, polymer- based redox-flow battery using

non-corrosive, safe, and low-cost materials. *Nature* **2015**, *527*, 78. doi: 10.1038/nature15746

(5) Ponce de León, C.; Frías-Ferrer, A.; González-García, J.; Szánto, D. A.; Walsh, F. C., Redox flow cells for energy conversion. *J. Power Sources* **2006**, *160*, 716. https://doi.org/10.1016/j. jpowsour. 2006. 02.095

(6) Kear, G.; Shah, A.; Walsh, F., Development of the all-vanadium redox flow battery for energy storage: A review of technological, financial and policy aspects. *Int. J. Energy Res*. **2012**, 36, 1105 https://doi.org/ 10.1002/er.1863

(7) Li, L.; Kim, S.; Wang, W.; Vijayakumar, M.; Nie, Z.; Chen, B.; Zhang, J.; Xia, G.; Hu, J.; Graff, G,. A stable vanadium redox-flow battery with high energy density for large-scale energy storage. *Adv. Energy Mater*. **2011**, *1*, 394. https://doi.org/10.1002/aenm.201100008

(8) Leung, P.; Li, X.; Ponce de León, C.; Berlouis, L.; John Low, C. T.; Walsh, F., Progress in redox flow batteries, remaining challenges and their applications in energy storage. *RSC Adv*. **2012**, *2*, 10125. doi: https://doi.org/10.1039/C2RA21342G

(9) Nikiforidis, G.; Berlouis, L.; Hall, D.; Hodgson, D., An electrochemical study on the positive electrode side of the zinc–cerium hybrid redox flow battery. *Electrochim. Acta* **2014**, *115*, 621. https://doi.org/ 10.1016/j.electacta.2013.09.081

(10) Nikiforidis, G.; Berlouis, L.; Hall, D.; Hodgson, D., Evaluation of carbon composite materials for the negative electrode in the zinc–cerium redox flow cell. *J. Power Sources* **2012**, *206*, 497. https://doi.org/10.1016/j.jpowsour.2011.01.036

(11) Leung, P.; Ponce de León, C.; Walsh, F., An undivided zinc–cerium redox flow battery operating at room temperature (295 K). *Electrochem. Commun*. **2011**, *13*, 770. https://doi.org/10.1016/j.elecom. 2011.04.011

(12) Leung, P.; Ponce-de-León, C.; Low, C. T. J.; Walsh, F., Zinc deposition and dissolution in methane sulfonic acid onto a carbon composite electrode as the negative electrode reactions in a hybrid redox flow battery. *Electrochim. Acta*. **2011**, *56*, 6536. https://doi.org/10.1016/ j.electacta .2011.04.111

(13) Li, Z.; Li, S.; Liu, S.; Huang, K.; Fang, D.; Wang, F.; Peng, S., Electrochemical properties of an all-organic redox flow battery using 2,2,6,6-tetramethyl-1-piperidinyloxy and N-methylphthalimide. *Electrochem. Solid-State Lett.* **2011**, *14*, A171. DOI:10.1149/2.012112ESL

(14) Yang, B.; Hoober-Burkhardt, L.; Wang, F.; Prakash, G.; Narayanan, S., An inexpensive aqueous flow battery for large-scale electrical energy storage based on water-soluble organic redox couples. *J. Electrochem. Soc*. **2014**, *161*, A1371. DOI 10.1149/2.1001409jes

(15) Alt, H.; Binder, H.; Köhling, A.; Sandstede, G., Investigation into the use of quinone compounds for battery cathodes. *Electrochim. Acta*. **1972**, *17*, 873. https://doi.org/10.1016/0013-4686(72)90010-2

(16) Wang, W.; Xu, W.; Cosimbescu, L.; Choi, D.; Li, L.; Yang, Z., Anthraquinone with tailored structure for a nonaqueous metal–organic redox flow battery. *Chem. Commun*. **2012**, *48*, 6669. DOI: https://doi.org/ 10.1039/C2CC32466K

(17) Wawzonek S.; Berkey. R.; Blaha, E. W.; Runner, M. E., Polarographic studies in acetonitrile and dimethyl-formamide, III. Behavior of quinones and hydro-quinones. *J. Electrochem. Soc*. **1956**, *103*, 456. DOI**:**10.1149/1.2430379.

(18) Davis, K.; Hammond, P.; Poever, M., Electron affinities of monosubstituted benzoquinonestrans. faraday soc. **1965**, *61*, 1516. https://doi.org/10.1039/TF9656101516

(19) Haimerl,A.; Merz, A., Catalysis of quinone-hydro-guinone redox reactions at polypyrrole benzene-sulphonate-coated platinum electrodes. *J. Electroanal. Chem*. **1987**, *220*, 55. https://doi.org/10.1016/0022-0728(87)88004-X

(20) Bhatt, D.; Anbuchezian, M.; Balasubramanian, R.; Udhayan. R.; Venkatesan, V. K. Cyclic voltammetric study of quinone—hydroquinone organic system in aqueous magnesium perchlorate electrolyte. *Journal of Power Sources*. **1993**, *45*, 177. https://doi.org/10.1016/0378-7753(93)87007-P

(21) Maruo, Y. Y.; Maruno, T., Tetrathiafulvalene–tetracyanoquinodimethane thin films grown by physical vapor deposition: Influence of substrate structures and substrate materials. Thin Solid Films. **2014**, *554*, 141. http://dx.doi.org./10.1016/j.tsf.2013.04.097

(22) Glicksman, R.; Morehouse, C., Investigation of the electrochemical characteristics of organic compounds, IV: Quinone Compounds. *J. Electrochem. Soc.* **1959**, *106*, 741.XWFwaFT65. DOI**:**10.1149/1.2427489

(23) Arsem,W.; US Patent No. 23 06 927. 1942

(24) Tripler, A.; McGreaw, L., An investigation of some new cathode depolarirer materials. *J. Electrochem. Soc*. **1958**, *105*, 179.

(25) Capson, A.; Parsons, R., The rate of a simple electron exchange reaction as a function of the electrode material. *J. ElectroanaL Chem*. **1973**, *46*, 215. https://doi.org/10.1016/S0022-0728(73)80130-5

(26) Quan, M.; Sanchez, D.; Wasylkiw, M. F.; Smith, D. K. Voltammetry of quinones in unbuffered aqueous solution: Reassessing the roles of proton transfer and hydrogen bonding in the aqueous electrochemistry of quinones. *J. Am. Chem. Soc*. **2007**, *129*, 42. 12847. https://doi.org/10.1021 /ja0743083

(27) Bogeski, I.; Gulaboski, R.; Kappl, R.; Mirceski, V.; Stefova, M.; Petreska, J.; Hoth, M., Calcium binding and transport by coenzyme Q. *J. Am. Chem. Soc*. **2011**, 133, 9293. DOI: 10.1021/ja110190t

(28) Gulaboski, R.; Markovski, V.; Jihe, Z., Redox chemistry of coenzyme Q–A. Short overview of the voltammetric features. *J. Solid State Electrochem*. **2016**, *20*, 3229. https://doi.org/10.1007 /s10008016-3230-7

(29) Gulaboski, R. The future of voltammetry. *Maced. J. Chem. Chem. Eng*. **2022**, *41*. DOI: 10.20450/mjcce.2022.2555

(30) Gulaboski1, R.; Mirceski, V., Application of voltammetry in biomedicine – recent achievements in enzymatic voltammetry. *Maced. J. Chem. Chem. Eng*. **2020**, *39*, 153. DOI:10.20450/mjcce.2020.2152

(31) Mirceski, V.; Gulaboski, R. Recent achievement in square-wave voltammetry. A review, *Maced. J. Chem. Chem. Eng*. **2014**, *33*, 1. DOI: https://doi.org/10.20450/mjcce.2014.515

(32) Soriaga, M.; Hubbard, A., Determination of the orientation of adsorbed molecules at solid-liquid interfaces by thin-layer electrochemistry: aromatic compounds at platinum electrodes. *J. Am. Chem. Soc*. **1982**, *104*, 2735. https://doi. org/ 10. 1021/ ja00374a008

(33) Nicholson, R.; Shain., Theory of stationary electrode polarography for a chemical reaction coupled between two charge transfers. *Anal. Chem.* **1965**, 37, 178. https://doi.org/10.1021/ac60221a002

(34) EL-Hallag, I.; Asiri, A.; EL-Mossalamy, E., Data analysis and evaluation of the electro-chemical parameters for the ET process via convolutive voltammetry and digital simulation. *J. Chil. Chem. Soc*. **2013**, *58*, 1920. http://dx.doi.org/10.4067/S0717-97072013000300028

(35) Bard, A.; Faulkner, L., *Electrochem. Methods*, John Wiley & Sons, New York, 1980

(36) Al-Owais, A.; El-Hallag, I.; El-Mossalamy, E., Electrochemical investigation of anthracen-9-ylmethylene-(3,4-dimethyl-isoxazol-5-yl)-amine compound at gold electrode. *Int. J. Electrochem. Sci*. **2022**, *17*, 220917. DOI:10.20964/2022.09.19

(37) Leddy, J.; Bard, A., Polymer films on electrodes. Part XVIII: Determination of heterogeneous electron transfer kinetics at poly(vinylferrocene) and nafion/Ru(bpy)$^{2+}{}_3$ polymer-modified electrodes by convolution voltammetry. *J. Electrolanal. Chem*. **1985**, *189*, 203. https://doi.org/ 10.1016/0368-1874(85)80068-X

(38) Oldham, K., Convolution of voltammograms as a method of chemical analysis. *J. Chem. Soc. Faraday Trans*. **1986**, *82*, 1. 1099–1104. https://doi.org/10. 1039/F19868201099

(39) Al-Owais, A.; El-Hallag, I.; El-Mossalamy, E., Voltammetric investigation of electrooxidation of methyl(E)-2-cyno(N-ethyl carbazol-2-yl) acrylate at a gold electrode. *Int. J. Electrochem. Sci*. **2022**, *17*, 220821. DOI: 10.20964/ 2022.08.08

(40) Guo,Y.; He, D.; Xie, A.; Qu, W; Tang, Y.; Zhou, L.; Zhu, R., The electrochemical oxidation of hydroquinone and catechol through a novel poly-geminal dicationic ionic liquid (PGDIL)–TiO_2 composite film electrode. *Polymers*. **2019**, *11*, 1907. https://doi.org/10.3390/polym11111907

(41) Bhatt, D.; Anbuchezian, M.; Balasubramanian, R.; Udhayan, R.; Venkatesan, V., Cyclic voltammetric study of quinone-hydroquinone organic system in aqueous magnesium perchlorate electrolyte. *J. Power Sources*. **1993**, *45*, 177. 10.1016/0378-7753(93)87007-P

(42) Yousofian-Varzaneh, H.; Zare, H. R.; Namazian, M. Application of tetrafluoro-p-hydroquinone and 3-fluorocatechol as the catholyte and cd nanoparticles as anolyte electroactive materials to manufacture of hybrid redox flow batteries. *J. Electroanal. Chem*. **2016**, *776*, 193. https://doi.org/10.1016/j.jelechem.2016.07.019

(43) Lopez da Silva, A. R.; Santos, A.; Martinez-Huitle, C. A. Electrochemical measurements and theoretical studies for understanding the behavior of catechol, resorcinol and hydroquinone on the boron doped diamond surface. *R.S.C. Adv*. **2018**, *8*, 3483. https://doi.org/10.1039/C7R-A12257